Predicting Monochrome Color Transmittance Spectra of Electrophotographic Prints

***Safer Mourad*[*], *Patrick Emmel*[**] *and Roger David Hersch*[**]**
[*]Eidgenössische Materialprüfungs- und Forschungsanstalt (EMPA)
[**]Ecole Polytechnique Fédérale de Lausanne (EPFL)

Abstract

We create a computer based numerical model to predict the color spectra of printed patches on dry toner electrophotographic printers. The goal of this research is to obtain a simplified model describing the input-output behavior of the printers based on the physical characteristics of the different printing process steps and the interactions between them. This leads to a better understanding of the factors that have an impact on printing quality. Furthermore, by modeling the non-linearities of the electrophotographic process, the prediction model will allow the creation of device calibration data with a minimal effort.

In order to avoid the additional optical non-linearities produced by light reflections on paper (dot-gain), we have limited the present investigation to transparency prints. In its current version, the proposed model is capable of predicting the transmittance spectra of a printed monochrome wedge down to a mean deviation less than CIELAB $\Delta E^*_{ab} = 1.5$.

The proposed simulation incorporates sub-models of the electrophotographic process [1, 2] shown in Fig. 1, such as the exposure of the photoreceptor, the generated electrostatic field, the toner's charge and diameter distributions, as well as the transfer and the fusing steps.

1. Introduction

The main difficulty in estimating the color in electrophotography is the high distortion of the printed dots and the large area where the neighboring effects can't be neglected. In spite of the printed dot distortion, virtually all classical color prediction models are still based on the assumption that the print consist of uniform dots with either a soft or even a hard dot density profile.

Observed under the microscope the general shape of electrophotographically printed dots are mostly like clouds of randomly distributed, more or less uniform colored toner particles. In general, these particles are spread beyond their theoretical target area which leads to extremely ragged edges. And finally, even the non printed image areas can be randomly covered by small toner particles looking like background noise.

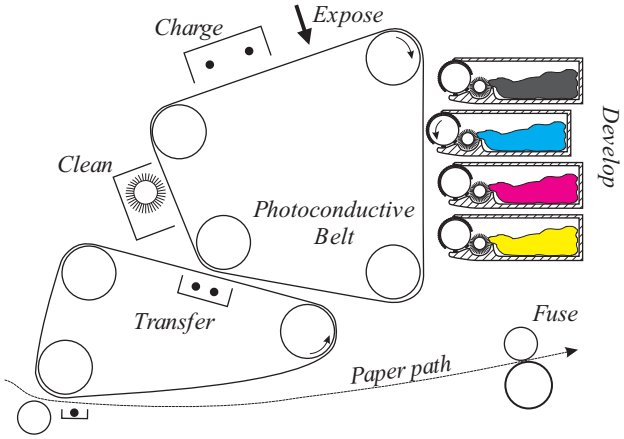

Figure 1: *The electrophotographic process.*

2. Modeling electrophotographic dots, monochrome prints and their spectra

To account for the mentioned prediction difficulties it is essential to take the microscopic density modulation into account. This is done by basing the predictions on an image analysis and processing approach at a microscopic scale. The basic idea of the prediction model is to simulate the density modulation of the electrophotographic printer by starting from the input page bitmap. The final goal is to match the predicted with the measured color spectra of a printed gradient.

The investigated printer has an addressability of $600dpi$. To simulate the micro density distribution of the prints, a high resolution grid is introduced comprising 42×42 *input bitmap elements* ($dots$). The chosen grid-spacing of $6.0\mu m$ represents a lower average size of a single toner particle. This leads to an image forming a square patch of $1.76 \times 1.76mm$ consisting of 294×294 high resolution *pixels*.

The formed image is passed from one sub-model to an other to simulate the effect of each significant process step. The methods presented in this paper are illustrated step by step on the base of Fig. 2. It shows a $210 \times 210 \mu m$ magnified section of a bitmap with a printing intensity of 32%.

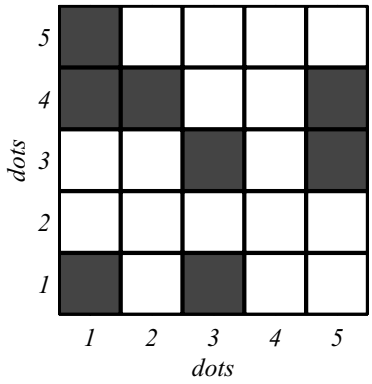

Figure 2: *Enlarged section of a printed bitmap.*

The surface of the electrophotographic plate is assumed to be homogeneously charged in the charging step. This surface charge is considered to be neither dependent on the current bitmap nor on the previously printed ones. Therefore, to predict the monochrome color spectra, the first significant process step is the constitution of the electrostatic field formed by the latent bitmap image.

2.1. Modeling the electrostatic field of a latent image

Past investigations have shown that the density of the electrophotographic images is essentially given by the perpendicular component of the electrostatic field above the photoconductive plate. Neugebauer [3, eq. 4-5] introduced $C(k)$ *Describing Function*, D.F., given in the following eq. 1 relating the perpendicular component of the electrostatic field to the exposure in the presence of a development electrode. In his later work[4] he justified the approximate usage of the D.F as a *Modulation Transfer Function*, MTF, for pictorial electrophotography.

$$C(k) = \frac{A(k)}{B(k)} \cosh(k(L_1 - z)) \quad (1)$$

where:

$$A(k) = \sinh(kL_2) - \frac{\beta}{kL_2}(\cosh(kL_2) - e^{-\beta})$$

$$B(k) = (\cosh(kL_1)\sinh(kL_2) + \cdots \eta \sinh(kL_1)\cosh(kL_2))(1 - (\frac{\beta}{kL_2})^2)$$

k : exposed line frequency
L_2 : thickness of the electrophotographic plate
L_1 : distance between the development electrode and the plate
β : function of L_2, drift mobility, trapping time and the initial plate voltage
η : dielectric constant of the plate
z : average distance of the charges above the plate.

The MTF $C(k)$ was initially developed to describe the field assuming an exposure made by a superposition of sinusoidal lines. However, we apply this MTF to approximate a convolution kernel $E_z(u, v)$ describing the perpendicular field component of a single exposed dot in the proximity of a development electrode; assuming an exposure $I(x)$ with a saturated Gaussian intensity profile based on [1, eq. 5.5]:

$$I(x) = \begin{cases} \tau_{exp} & : x \in [\, x_1, x_2 \,] \\ I_0 e^{-0.5(x/\alpha)^2} & : \text{otherwise} \end{cases} \quad (2)$$

where

x : spatial coordinate ($= 1/2\pi k$)
τ_{exp} : saturation
x_1, x_2 : solution of the relationship $I(x) = \tau_{exp}$
I_0, α : constants dependent on the exposure unit.

With $c(x)$, the inverse *Fourier-Transform* of the MTF $C(k)$, the line convolution kernel $E_z(x)$ can than be written as:

$$E_z(x) = I(x) * c(x) \quad (3)$$

By substituting x with $\sqrt{u^2 + v^2}$, the line profile in eq. 3 leads to our approximation of the perpendicular component of the electrostatic field: the circular convolution kernel $E_z(u, v)$. An example of the resulting dot field approximation is shown in Fig. 3.

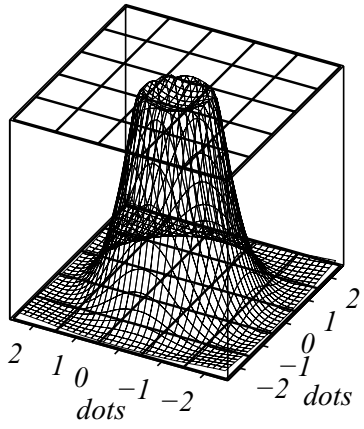

Figure 3: *Convolution kernel $E_z(u, v)$ used to model the perpendicular electrostatic field component of a single dot.*

Figure 4 further shows the electrostatic field of the latent image derived by the superposition of the exposed dot fields. This is done by using a convolution of $E_z(u,v)$ with a high resolution grid containing zeros except at the center of the exposed input bitmap dots.

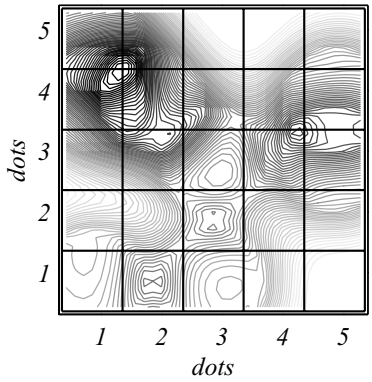

Figure 4: *Contour plot of the perpendicular component of the simulated electrostatic field. The plate is assumed to be imaged with the bitmap shown in Fig. 2.*

2.2. Modeling the developed and transferred image

In the developing step, the formed electrostatic latent image is developed in the vicinity of the developer roll with charged toner particles. Roughly, according to the Coulomb force, the electrostatic force is given by a linear relationship between the charge and the acting electrostatic field

$$\vec{F} = q\vec{E} \tag{4}$$

where
$\vec{F}$: electrostatic force
q : point charge
$\vec{E}$: electrostatic field.

For simplicity, it is assumed that the electrostatic force is essentially driven by the perpendicular electrostatic field component E_z and that development occurs as soon as the attracting electrostatic force is strong enough to overcome the impeding adhesion forces. In our simulation we substitute an unknown *threshold* τ_{imp} constant for the impeding adhesion forces; i.e. according to [2, eq. 9.1], development occurs when

$$qE_z > \tau_{imp} \tag{5}$$

Due to the grinding and charging process, the developed particles' size and charge are distributed in a statistical manner. The charge distribution definitely influences the development behavior, whereas the size distribution mainly affects the micro transmittance structure according to *Bouguer-Lambert's law* [5, p. 30-31] which we apply on a microscopic scale as follows:

$$\vartheta(\lambda) = \left[\vartheta_0(\lambda)\right]^{\frac{d}{d_0}} \tag{6}$$

where
λ : wavelength of light
ϑ, ϑ_0 : spectral transmittance of a new and a measured layer of the same color
d, d_0 : thickness of the new and the original layers.

If we refer $\vartheta_0(\lambda)$ to a transmittance spectrum of a solid patch $\vartheta_{100\%}(\lambda)$ measured using a macroscopic spectrophotometer, than d_0 would represent an average thickness of the fused toner layer. On a microscopic scale and under the condition that the color transmittance of the fused toner particles obeys the Bouguer-Lambert's law, eq. 6 can be written as:

$$\vartheta(\lambda) = \left[\vartheta_{100\%}(\lambda)\right]^{\delta} \tag{7}$$

with
δ : relative diameter of the toner particles.

In the presented simulations the distributions of the size and charge of the particles are assumed to be independent. The charges q are approximated by random numbers from a lognormal distribution having a *Probability Density Function*, pdf_q, like:

$$pdf_q(\kappa) = \gamma - \frac{1}{\kappa\,\sigma\sqrt{2\pi}}\, e^{\frac{-(\ln\kappa-\mu)^2}{\sigma^2}} \tag{8}$$

Whereas the pdf_δ of the relative particles diameter δ is based on the Rayleigh distribution:

$$pdf_\delta(\kappa) = a + \frac{\kappa}{b^2}\, e^{\frac{-\kappa^2}{2b^2}} \tag{9}$$

where
γ, σ, μ : constants dependent on the toner's charge characteristics
a, b : constants dependent on the toner's diameter characteristics

These distributions were selected to match the general shapes reported in various measurements found in literature (for example [6]). The development condition (eq. 5) is evaluated at each pixel of the simulation frame with a random charge according to pdf_q. If the condition is fulfilled, the pixel which initially equals zero, is replaced by a particle having a random diameter according to pdf_δ.

Since we restrict ourselves to the prediction of monochrome spectra, the transfer mechanism can be simplified and assumed as an independent process of the imaged bitmap. In this present investigation, the transfer step is modeled by rejecting randomly chosen toner particles from the previously transferred image. Figure 5 illustrates a simulation result of the developed and transferred latent image.

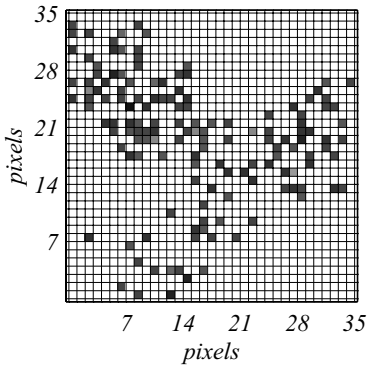

Figure 5: *Simulation of the developed and transferred toner particles. The gray levels indicates the diameter variations.*

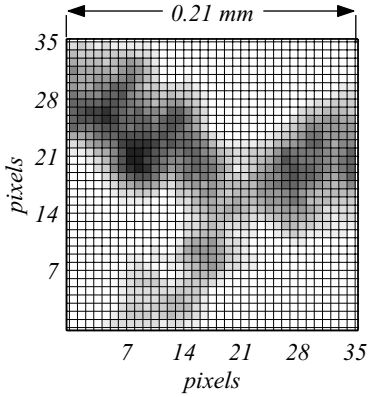

Figure 7: *Enlarged section of a simulated fused image.*

2.3. Modeling the fusing step

The main effects due to the fixing heat and pressure within the fuser nip, such as toner flow, spread, join and penetration etc., are simulated using a low pass filtering convolution kernel based on the following polynomial approach (see Fig. 6):

$$H(\rho) = \begin{cases} 1 - (\frac{\rho}{\sigma_f})^4 : \rho \in [\,-\sigma_f, \sigma_f\,] \\ 0 \quad\quad : \text{otherwise} \end{cases} \tag{10}$$

with

σ_f : average fuser spreading width.

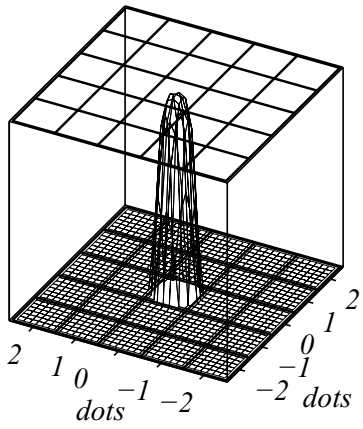

Figure 6: *Convolution kernel simulating the effect of the fuser on the transferred toner particles.*

The spreading width of the fuser is further considered to be dependent on the average gap size between the transferred particles. This imply that the spreading σ_f is a function of the printed bitmap.

2.4. Calculating the transmittance spectra

The obtained image of the last section consists of a thickness profile δ_i of the simulated fused bitmap. This profile can be converted to a transmittance spectra profile using eq. 7 directly. To collect this profile to a simulated spectrum $T(\lambda)$ which would be obtained by a macroscopic measuring spectrophotometer, the average of the simulated micro-spectra has to be taken as follows:

$$T(\lambda) = \frac{1}{N} \sum_{i=1}^{N} \left[\vartheta_{100\%}(\lambda)\right]^{\delta_i} \tag{11}$$

3. Experimental

Color wedges $[\,0\% - 100\%\,]$ consisting of sixty six intensities of each process color were printed on transparencies using a *Tektronix Phaser560 E*. The input bitmap of the patches were saved in numerical files to serve as simulation input for the predictions. The transmittance spectrum of each patch was measured with a *Gretag Spectroscan Transmission* measurement instrument.

From each color, up to five arbitrary chosen spectra were selected as a learning-set to fit the various model constants applying a constrained non-linear optimization, implemented in MATLAB [7]. The optimization goal was the average deviation between the measured and the simulated spectra in terms of CIELAB ΔE^*_{ab} [5, p. 166-168].

The model constants were optimized for each process color separately except the ones which are color independent. These color independent parameters, such as the ones of the exposure step were optimized using only the spectra of the Magenta wedge. Finally, after a completed optimization run, all optimized parameters were fixed and the model was tested using the testing-set consisting of the remaining sixty spectra of each color.

4. Prediction results

The prediction was tested twenty independent times while resetting each time the random generator to a different seed. Figure 8 shows a color deviation histogram illustrating the obtained prediction performance.

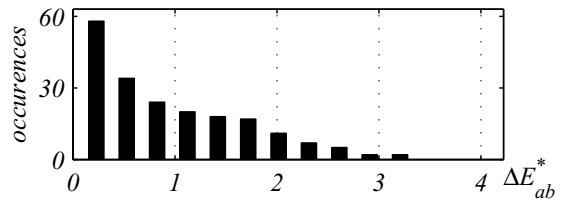

Figure 8: *Prediction performance histogram.*

The following table summarize the obtained prediction errors of each color separately. The process noise given in the last line, states the average color deviation between different measurements of the same patch. It is hard for the human eye to distinguish a color deviation in the range of the obtained mean prediction error. In addition, the upper limit of the obtained deviation is close to the level of the process noise.

Color	$\Delta E^*_{ab\ mean}$	$\Delta E^*_{ab\ max}$
Cyan	1.31	3.36
Magenta	0.84	2.83
Yellow	0.69	2.81
Process Noise	0.32	2.56

5. Conclusions

This investigation demonstrates a model based on a MTF and on randomized toner particles to simulate the developing electrostatic forces acting in electrophotographic printers. By applying at microscopic scale additional models for the transfer and the fusing steps, we obtain a simulation of the relative thickness profile of the fused toner particles.

The relative toner thickness is transformed to simulate color transmittance spectra permitting the optimization and evaluation of the model performance. At the moment, only five measured transmittance spectra of each process color are needed to fit the model parameters.

The achieved color prediction method can be considered as a simplified printer simulation focused on the colorimetric significance of the involved electrophotographic process steps. During the optimization, no information about the effective toner distribution is provided. Yet, the resulting model is capable of approximating the microscopic image of the prints, as shown in Fig. 9.

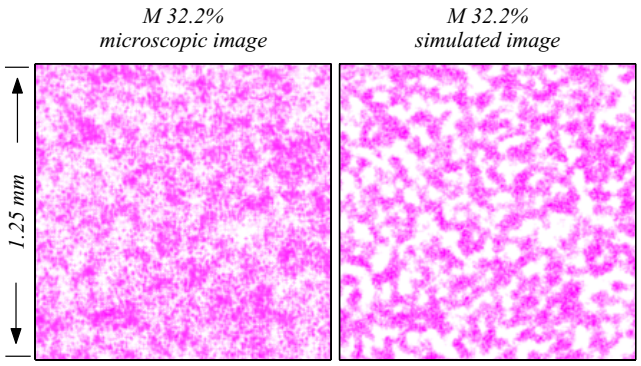

Figure 9: *Comparison between weakly magnified sections of a simulated and a true image of a printed magenta patch.*

6. Biography

Safer Mourad received the M.S. degree in electrical engineering in 1993 from the Swiss Federal Institute of Technology (ETH), Zurich. From 1993 to 1997, he developed real-time video tracking and high precision surveying instruments at Leica Geosystems. In January 1998 he joined the Media Technology Department at the EMPA, St. Gallen and is currently working towards his Ph. D. His research interests includes colorimetry, image processing and real-time control applications. He received the Swiss IEEE Award for his M.S. thesis and is a member of the IS&T.
E-mail address: safer.mourad@empa.ch

References

[1] E. M. Williams. *The Physics and Technology of Xerographic Processes*. John Wiley & Sons, Inc., 1984.

[2] L. B. Schein. *Electrophotography and Development Physics*. Laplacian Press, rev. 2. edition, 1996.

[3] H. E. J. Neugebauer. A describing function for the modulation transfer of xerography. *Applied Optics*, 4(4):453–459, 1965.

[4] H. E. J. Neugebauer. Development method and modulation transfer function of xerography. *Applied Optics*, 6(5):943–945, 1967.

[5] G. Wyszecki. *Color Science*. John Wiley & Sons, Inc., 2. edition, 1982.

[6] R. J. Nash, M. L. Grande, and R. N. Muller. The effect of toner and carrier composition on the average and distributed toner charge values. In *NIP14*, pages 332–340, Toronto, Ontario, 1998. IS&T.

[7] *Optimization Toolbox*. MathWorks, 1999.